ORNL/TM-2024/3431

CRADA NFE-22-09321 Final Report – Isothermal Compressor Computational Fluid Dynamics Simulations

Stephen Kowalski
Duy Thien Nguyen
Mingkan Zhang

August 2024

OAK RIDGE National Laboratory

ORNL IS MANAGED BY UT-BATTELLE LLC FOR THE US DEPARTMENT OF ENERGY

ORNL/TM-2024/3431

Buildings and Transportation Science Division

CRADA NFE-22-09321 FINAL REPORT – ISOTHERMAL COMPRESSOR COMPUTATIONAL FLUID DYNAMICS SIMULATIONS

Stephen Kowalski
Duy Thien Nguyen
Mingkan Zhang

August 2024

Prepared by
OAK RIDGE NATIONAL LABORATORY
Oak Ridge, TN 37831
managed by
UT-BATTELLE LLC
for the
US DEPARTMENT OF ENERGY
under contract DE-AC05-00OR22725

CONTENTS

LIST OF FIGURES

LIST OF ABBREVIATIONS

BTO	Building Technologies Office
CAD	Computer Aided Design
CBECS	Commercial Building Energy Consumption Survey
CFD	Computational Fluid Dynamics
CRADA	Cooperative Research and Development Agreement
MMP	Mixture Multi-Phase
ORNL	Oak Ridge National Laboratory
RANS	Reynolds-Averaged Navier–Stokes

ABSTRACT

Carnot Compression is a startup company developing an innovative technology for air and gas compression. This technology is inherently oil-free and isothermal due to the use of water to simultaneously compress and cool the gas throughout the process. Isothermal gas compression eliminates the need to cool the compressed gas so it may lead to significant energy savings. The development of Carnot's isothermal compressor is limited by the lack of insight into the flow and detailed behavior of the fluids (water and air/gas) inside the air end. Previous and current attempts at Computational Fluid Dynamics (CFD) simulations by Carnot have been unable to provide the level of accuracy required to use simulations for technology development. In this Cooperative Research and Development Agreement (CRADA) project, Oak Ridge National Laboratory (ORNL) used the CFD package Star-CCM+ to successfully develop a CFD simulation, providing the much-needed insight required to speed up the development. The work is intended to enable Carnot Compression to unlock its technology potential to a level sufficient for commercialization of the intended first product. The work will also prepare Carnot to scale the technology to much larger and more energy intensive applications, positioning it to broaden the product applications. Successful development of the technology has the potential to result in 20% or more efficiency gains for compression processes, or about $3 billion in annual energy savings potential for the U.S. alone.

1. STATEMENT OF OBJECTIVES

The objective of the project was to simulate a well-known and tested set of air end components with various CFD software suites and setup parameters to identify a combination that improves the accuracy of the CFD results and correlates well with the experiment.

2. BENEFITS TO THE BUILDING TECHNOLOGY OFFICE'S MISSION

Air compression is used in various commercial applications such as food and beverage production, light manufacturing, and equipment repair. Energy use attributed to air compressors falls under the "Other" end-use consumption in the 2018 Commercial Building Energy Consumption Survey (Commercial Building Energy Consumption Survey (CBECS)) (US Energy Information Administration, 2018), which accounts for 16% of total end-use consumption, so while air compression is a relatively small factor in energy use in commercial buildings, improvements of the amount suggested by Carnot can be compelling to reduce building energy use. Therefore, the development of more efficient technology for air compression fits well with the mission of Building Technologies Office (BTO) to enable high-performing, energy-efficient commercial buildings.

3. NUMERICAL STUDY

In this effort, Carnot Compression developed several compressor designs and requested technical assistance from ORNL to perform numerical modeling of those configurations. The main configurations of compressors developed by Carnot Compression that were analyzed in this project are the vortex and lambda designs, each with several minor modifications done by Carnot Compression during the project execution. This report presents the results of the analysis of the vortex design, while the following report presents the results of the analysis of the lambda design. In addition to sharing the Computer Aided Design (CAD) files with geometrical dimensions, Carnot Compression provided the operating and boundary conditions of each design configuration.

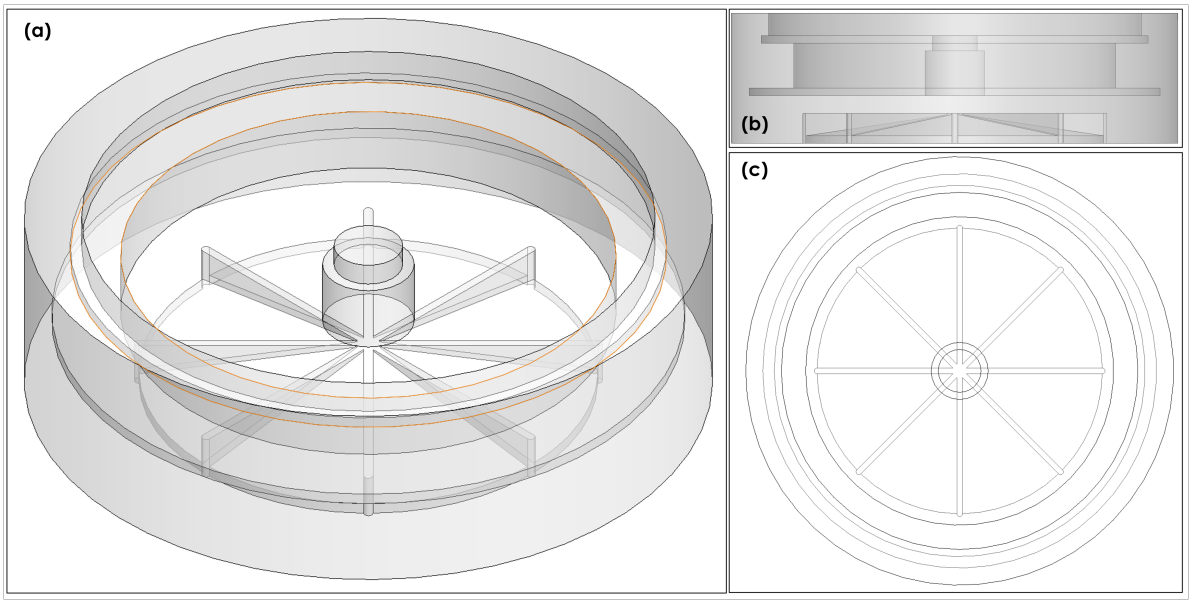

Figure 1. A CAD design of vortex-based compressor configuration, (a) isometric view, (b) side view, and (c) top view.

3.1 NUMERICAL MODELING OF A VORTEX DESIGN COMPRESSOR

This section describes the numerical modeling efforts of the vortex-designed compressor configuration. Carnot Compression supplied a CAD file of the vortex-based air compressor design (see Figure 1) to the ORNL team for preliminary examination and tests of meshing and modeling methodologies. An initial evaluation was performed to understand the feasibility of modeling the full domain of the design configuration with respect to the project timeline and funding. After discussions between the ORNL and Carnot Compression regarding the benefits and drawbacks of the computational effort required to analyze the full domain, a model containing a $1/6^{th}$ (60-degree angle) portion of the entire compressor was used to perform numerical calculations. Figure 2 illustrates the $1/6^{th}$ model configuration of the vortex compressor. In this design, water and air are supplied at the inlets and enter the flow domain. Due to the rotation applied, the mixture of air and water is subjected to centrifugal force and compressed. Because water and air have a significant density difference and the entering air is compressible, air and water will leave the domain at their corresponding outlets. From the harvest pockets, the compressed air is driven through the main shaft. Since the air is surrounded by water during the compression, the heat generated by the compression is immediately absorbed by the water. The result

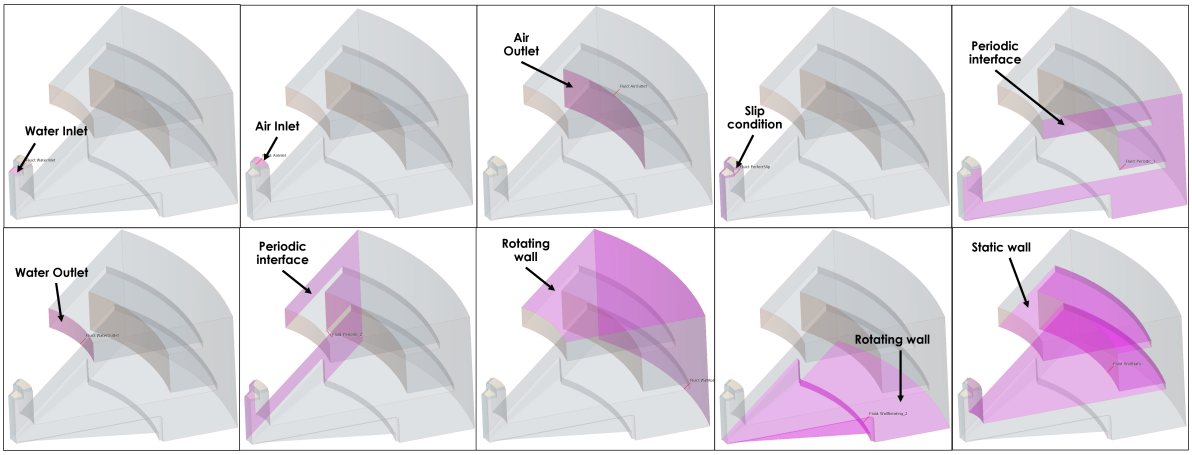

Figure 2. The 1/6th (60-degree angle) CAD design of vortex-based compressor configuration with boundary conditions highlighted.

is isothermal compression, which is potentially more efficient than incumbent technologies and produces naturally oil-free air.

Fully conformal meshes were generated using polyhedral and prism layer meshing operations. Mesh generation was performed using the automatic meshing capability in Star-CCM+. The Surface Remesher, Polyhedral Mesher, and Prism Layer Mesher were used (User Guide 2021). The Surface Remesher performed surface vertex re-tessellation of the imported 3D CAD to optimize surface faces based on the target edge length and proximity refinements. The Polyhedral Mesher utilized an arbitrary polyhedral cell shape in order to build the core mesh. The polyhedral meshes are efficient to build as they require no more surface preparation than the equivalent tetrahedral mesh. The polyhedral meshes also contain approximately five times fewer cells than a tetrahedral mesh for a given starting surface. In the Polyhedral Mesher process, a tetrahedral mesh is first generated for the input surface. Second, a dualization scheme is used to create the polyhedral mesh from the underlying tetrahedral mesh. The volume growth rate controls how quickly the cell size increases with increasing distance from the surface and from refinement zones to mesh away from the zones. The maximum cell size control sets the upper limit on how large cells can grow. The Prism Layer Mesher generated a subsurface to extrude a set of prismatic cells from region surfaces into the core mesh. This layer of cells is necessary to improve the accuracy of the flow solution. Figure 3 shows the computational mesh generated for the numerical simulation of the 1/6th domain of vortex-based compressor configuration.

The modeling effort of the vortex-based compressor design configuration started first with the steady Reynolds-Averaged Navier–Stokes (RANS) equations to model the heat-transfer and fluid-flow physics and coupled with the segregated flow and segregated multiphase temperature models for energy and flow transport. The realizable k-ϵ turbulence model and two-layer all y^+ wall treatment were chosen. The turbulent fluid motion is governed by the conservation of mass, linear momentum, and energy, given as follows.

$$\frac{\partial \rho}{\partial t} + \nabla \cdot (\rho \boldsymbol{v}) = 0, \tag{1}$$

where ρ is the density, and v is the continuum velocity.

$$\frac{\partial (\rho \boldsymbol{v})}{\partial t} + \nabla \cdot (\rho \boldsymbol{v} \otimes \boldsymbol{v}) = -\nabla \cdot (p\boldsymbol{I}) + \nabla \cdot \boldsymbol{T} + \boldsymbol{f}_b, \tag{2}$$

where $\otimes$ denotes the outer product, f_b is the resultant of the body forces per unit volume acting on the continuum, and σ is the stress tensor. For a fluid, the stress tensor is often written as the sum of normal

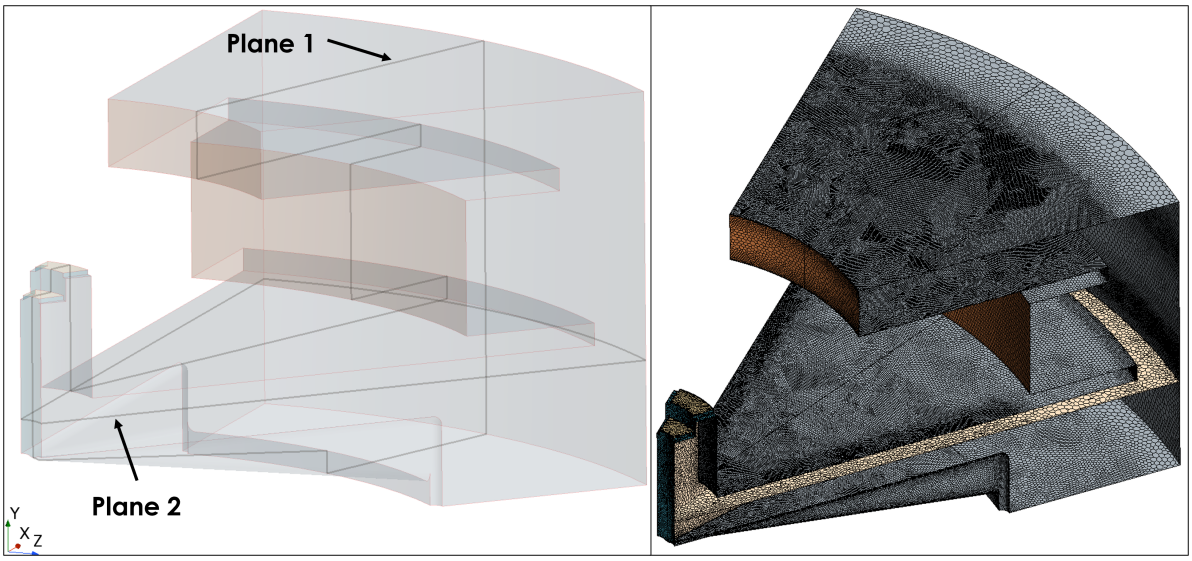

Figure 3. (Left) A CAD design of 1/6th domain of vortex-based compressor configuration and (right) computational mesh generated for the numerical simulation.

stresses and shear stresses, $\sigma = -p\boldsymbol{I} + \boldsymbol{T}$, where p is the pressure, and $\boldsymbol{T}$ is the viscous stress tensor.

$$\frac{\partial(\rho E)}{\partial t} + \nabla \cdot (\rho E \boldsymbol{v}) = \boldsymbol{f}_b \cdot \boldsymbol{v} + \nabla \cdot (\boldsymbol{v} \cdot \boldsymbol{\sigma}) - \nabla \cdot \boldsymbol{q} + \boldsymbol{S}_E, \tag{3}$$

where E is the total energy per unit mass, q is the heat flux, and S_E is an energy source per unit volume. The RANS-based approach to turbulence modeling was chosen for this study due to its relatively low computational cost compared to large-eddy simulation, and direct numerical simulation. The temporal averaging methodology, or decomposition process, was to split fluid variables into their time-averaged means and fluctuating components.

To obtain the RANS equations, each solution variable ϕ in the instantaneous Navier-Stokes equations is decomposed into its mean, or averaged, value $\bar{\phi}$ and its fluctuating component ϕ':

$$\phi = \bar{\phi} + \phi' \tag{4}$$

where ϕ represents velocity components, pressure, energy, or species concentration. Applying this process to the above three equations yields

$$\frac{\partial \rho}{\partial t} + \nabla \cdot (\rho \bar{\boldsymbol{u}}) = 0 \tag{5}$$

$$\frac{\partial}{\partial t}(\rho \bar{\boldsymbol{u}}) + \nabla \cdot (\rho \bar{\boldsymbol{u}} \otimes \bar{\boldsymbol{u}}) = -\nabla \cdot (\bar{p}\boldsymbol{I}_t) + \nabla \cdot (\bar{\tau} + \tau_{RANS}) + \boldsymbol{F_b} \tag{6}$$

where ρ is the density, I_t is the identity tensor, $\bar{\boldsymbol{u}}$ is the mean velocity vector, $\bar{p}$ the mean pressure, $\bar{\tau}$ is the mean viscous stress tensor and τ_{RANS} is the Reynolds stress tensor. The correlation between the fluctuating velocities is represented by the Reynolds stress tensor, $< u_i u_j >$, which is an unknown term, and a closure problem is required to model this stress tensor. One closure approach is based on eddy-viscosity models, which uses the concept of a turbulent eddy viscosity μ_t to model the stress tensor as a function of mean flow quantities. The most common model is known as the Boussinesq approximation:

$$\tau_{RANS} = 2\mu_t \boldsymbol{S} - \frac{2}{3}(\mu_t \nabla \cdot \bar{\boldsymbol{v}})\boldsymbol{I} \tag{7}$$

where $\boldsymbol{S}$ is the mean strain rate tensor given by

$$\boldsymbol{S} = \frac{1}{2}\left(\nabla\bar{\boldsymbol{v}} + \nabla\bar{\boldsymbol{v}}^T\right) \tag{8}$$

and $\bar{\boldsymbol{v}}$ is the mean velocity.

In this study, the applied closure method is the realizable k-ϵ model containing a new transport equation for the turbulent dissipation rate ϵ (User Guide 2021). The k-ϵ turbulence model is a two-equation model that solves transport equations for the turbulent kinetic energy k and the turbulent dissipation rate ϵ to determine the turbulent eddy viscosity. Various forms of the k-ϵ model have been incorporated into Simcenter STAR-CCM (User Guide 2021). According to the recommendations from STAR-CCM+ user's manual, the realizable k-ϵ (Shih et al. 1995) is known to be very stable and perform substantially better than the standard k-ϵ model (Jones and Launder 1972) for many applications. It contains a new transport equation for the turbulent dissipation rate ϵ and a variable damping function f_μ, which is expressed as a function of mean flow and turbulence properties, is applied to a critical coefficient of the model C_μ. This new approach allows the model to satisfy certain mathematical constraints on the normal stresses consistent with the physics of turbulence (realizability) (User Guide 2021). A two-layer wall treatment (Rodi 1991) was employed in combination with the realizable k-ϵ model. The two-layer approach facilitates the realizable k-ϵ model to be applied in the viscous-affected layer (including the viscous sub-layer and the buffer layer). In Simcenter STAR-CCM+, the two-layer formulations work with either wall-function type meshes $y^+ > 30$ when the mesh is not fine enough to solve the near-wall boundary layer or low-Reynolds number type meshes $y^+ \approx 1$ when the mesh is fine enough to discretize the sub-viscous layer near the wall. The transport equations for the kinetic energy k and the turbulent dissipation rate ϵ are

$$\frac{\partial}{\partial t}(\rho k) + \nabla\cdot(\rho k\bar{\boldsymbol{v}}) = \nabla\cdot\left[\left(\mu + \frac{\mu_t}{\sigma_k}\right)\nabla k\right] + P_k - \rho(\epsilon - \epsilon_0) + S_k \tag{9}$$

$$\frac{\partial}{\partial t}(\rho\epsilon) + \nabla\cdot(\rho\epsilon\bar{\boldsymbol{v}}) = \nabla\cdot\left[\left(\mu + \frac{\mu_t}{\sigma_\epsilon}\right)\nabla\epsilon\right] + \frac{1}{T_\epsilon}C_{\epsilon1}P_\epsilon - C_{\epsilon2}f_2\rho\left(\frac{\epsilon}{T_e} - \frac{\epsilon_0}{T_0}\right) + S_\epsilon \tag{10}$$

where $\boldsymbol{v}$ is the mean velocity, μ is the dynamic viscosity, σ_k, σ_ϵ, $C_{\epsilon1}$, and $C_{\epsilon2}$ are model coefficients, P_k and P_ϵ are production terms, f_2 is a damping function, and S_k and S_ϵ are the user-specified source terms. The realizable k-ϵ models provide a good compromise between robustness, computational cost and accuracy. They are generally well suited to industrial-type applications that contain complex recirculation, with or without heat transfer.

Following the discussions and experiences shared by Carnot Compression, the Mixture Multi-Phase (MMP) model is considered to model the multiphase flow phenomena occurring within the simulation domain. According to StarCCM+ user manual (User Guide 2021), in the MMP model, mass, momentum, and energy are treated as mixture quantities rather than phase quantities. Simcenter STAR-CCM+ solves transport equations for the mixture as a whole, and not for each phase separately. To calculate the distribution of phases, the volume fraction transport equation is solved for each phase. For phases that are moving at different velocities, algebraic relations are used to compute the relative velocities. The MMP model is computationally more efficient than models that simulate each phase separately. **In STAR-CCM+, when the MMP model is selected, the segregated multiphase temperature model can be used optionally to control the thermal effects in the simulations. The segregated multiphase temperature model solves the total energy equation with temperature as the solved variable (User Guide 2021). In this study, as the segregated multiphase temperature model is selected, the specific heat of mixture is estimated using the mass-weighted mixture method, which calculates a given mixture property by mass-weighting the**

component property values. For example, mixture property ϕ_{mix} is

$$\phi_{mix} = \sum_{i=1}^{N} y_i \phi_i \tag{11}$$

where y_i and ϕ_i are the mass fraction and property values of mixture component-i and N is the total number of components in the mixture.

The volume fractions are transported according to the following conservation equation:

$$\frac{\partial}{\partial t}\int_V \alpha_i dV + \int_A \alpha_i \boldsymbol{v}_m \cdot d\boldsymbol{a} = \int_V \left(S_{u,i} - \frac{\alpha_i}{\rho_i}\frac{D\rho_i}{Dt} \right) dV + \int_A \frac{\mu_t}{\sigma_t \rho_m} \nabla \alpha_i \cdot d\boldsymbol{a} - \int_V \frac{1}{\rho_i} \nabla \cdot (\alpha_i \rho_i \boldsymbol{v}_{d,i})\, dV \tag{12}$$

where:

- t is time
- V is volume
- α_i is the volume fraction of phase i
- $\boldsymbol{v}_m$ is the mass-averaged velocity
- $\boldsymbol{a}$ is the surface area vector
- $S_{u,i}$ is the user-defined source term for phase
- ρ_i is the density of phase i
- μ_i is the turbulent dynamic viscosity
- σ_t is the turbulent Schmidt number
- $\boldsymbol{v}_{d,i}$ is the diffusion velocity.

The conservation of mass for the mixture of phases is given by:

$$\frac{\partial}{\partial t}\int_V \rho_m dV + \int_A \rho_m \boldsymbol{v}_m \cdot d\boldsymbol{a} = \int_V S_u dV \tag{13}$$

where:

- ρ_m is the density of the mixture
- S_u is a user-defined mass source term

The momentum balance for the mixture of phases is given by:

$$\frac{\partial}{\partial t}\int_V \rho_m \boldsymbol{v}_m dV + \int_A \rho_m \boldsymbol{v}_m \otimes \boldsymbol{v}_m \cdot d\boldsymbol{a} = -\int_A p\boldsymbol{I} \cdot d\boldsymbol{a} + \int_A \boldsymbol{T}_m \cdot d\boldsymbol{a} + \int_V \boldsymbol{f}_b dV + \int_V \boldsymbol{s}_u dV - \sum_i \int_A \alpha_i \rho_i \boldsymbol{v}_{d,i} \otimes \boldsymbol{v}_{d,i} \cdot d\boldsymbol{a} \tag{14}$$

where:

- $\boldsymbol{I}$ is the unity tensor
- p is pressure
- $\boldsymbol{T}_m$ is the viscous stress tensor
- $\boldsymbol{f}_b$ is the body force vector

- $\boldsymbol{s}_u$ is a user-defined momentum source term.

The stress tensor, $\boldsymbol{T}_m$, is estimated as:

$$\boldsymbol{T}_m = \mu_{eff}\left[\left(\nabla \boldsymbol{v}_m + (\nabla \boldsymbol{v}_m)^T\right) - \frac{2}{3}(\nabla \cdot \boldsymbol{v})\,\boldsymbol{I}\right] \tag{15}$$

where μ_{eff} is the effective viscosity.

The energy equation for the mixture of phases reads:

$$\frac{\partial}{\partial t}\int_V \rho_m E_m dV + \int_A \left(\rho_m H_m \boldsymbol{v}_m + \sum_i \alpha_i \rho_i H_i \boldsymbol{v}_{d,i}\right)\cdot d\boldsymbol{a} = -\int_A \dot{\boldsymbol{q}}\cdot d\boldsymbol{a} + \int_A \boldsymbol{T}_m \cdot \boldsymbol{v}_m \cdot d\boldsymbol{a} + \int_V (\boldsymbol{f}_b \cdot \boldsymbol{v}_m + S_u)\,dV \tag{16}$$

where:

- E_m is the total energy of the mixture
- H_m is the total enthalpy of the mixture
- $\dot{\boldsymbol{q}}$ is the heat flux vector
- S_u is a user-defined energy source term

Total energy E_m and total enthalpy H_m of the mixture are defined as:

$$E_m = H_m - \frac{p}{\rho_m}, \tag{17}$$

$$H_m = h_m - \frac{|\boldsymbol{v}_m|^2}{2} \tag{18}$$

where h_m is the mixture-specific static enthalpy. The mixture quantities in the above equations are defined as follows.

- Density: $\rho_m = \sum_{i=1}^{n} \rho_i \alpha_i$
- Viscosity: $\mu_m = \sum_{i=1}^{n} \mu_i \alpha_i$
- Velocity: $\boldsymbol{v}_m = \frac{1}{\rho_m}\sum_{i=1}^{n} \boldsymbol{v}_i \alpha_i \rho_i$
- Thermal Conductivity: $k_m = \sum_{i=1}^{n} k_i \alpha_i$
- Enthalpy: $H_m = \frac{1}{\rho_m}\sum_{i=1}^{n} h_i \alpha_i \rho_i + \frac{|\boldsymbol{v}_m|^2}{2}$

Carnot Compression suggested boundary conditions applied to the numerical modeling of vortex compressor as follows.

- A rotating reference frame is applied, and the rotational speed gradually increased from 100, 300, 600, 1300, and 1750, to a maximum 2600 RPM to stabilize the calculations.
- Air Inlet is assigned with the mass flow rate which gradually increased from 0.026 g/s to 0.687 g/s.
- Air Outlet is assigned with the pressure outlet which relative pressure gradually increased from 1173 Pa to 793103 Pa.
- Water Inlet is assigned with the mass flow rate which gradually increased from 6.98 g/s to 181.6 g/s.
- Water Outlet is assigned with a pressure outlet of 0 Pa relative pressure.

The numerical simulations were performed using the physics models and settings described above. The calculations started with lower rotational speed, mass flow rates, and pressures. Then, these boundary conditions were gradually increased until reaching 2600 RPM. Results obtained from the CFD calculations for 2600 RPM are depicted in Figures 4 and 5. Results depicted in Figures 4 and 5 revealed that with the current boundary conditions applied at the domain inlets and outlets, air and water entered the domain via their corresponding inlets separately making a small pocket of air in the vicinity of the water and air inlets. In addition, a large pressure difference between the air outlet and water outlet created a pressure-driven air flow as can be seen in Figure 5(c). This internal flow pattern between the outlets forced the mixture of air and water to stay within the lower volume of the domain. Results were presented and shared with the industry partner, Carnot Compression, over several meetings to discuss the outcomes and potential modifications on the design operating and boundary conditions. It is concluded that maximum values of air and water mass flow rates, and air outlet pressure are not realistic.

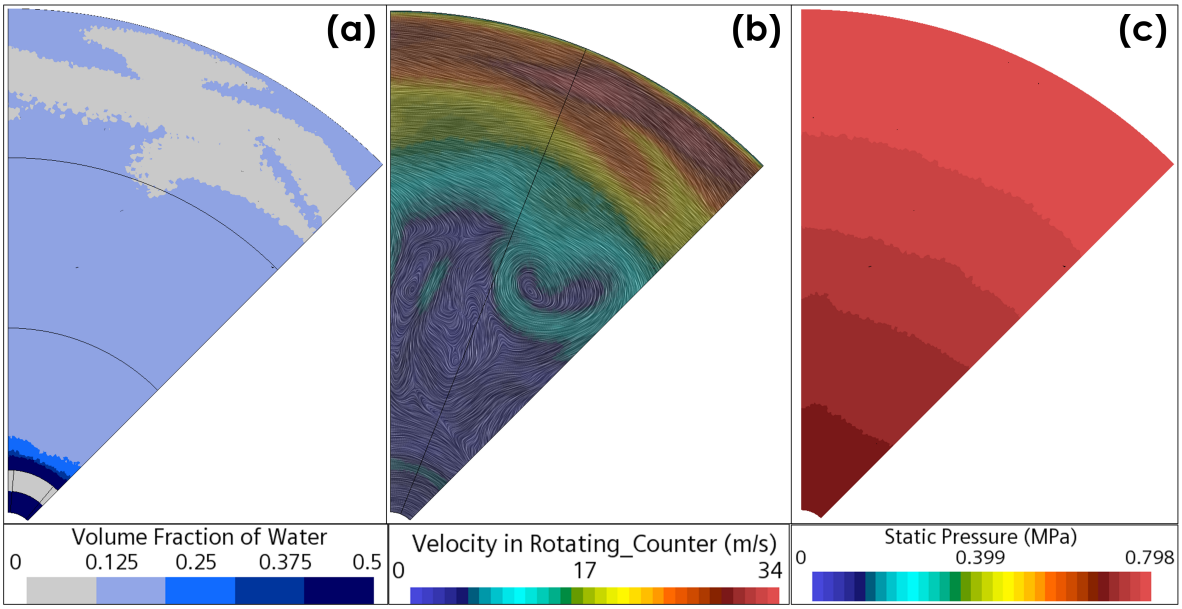

Figure 4. Results obtained from CFD calculations of the 1/6th domain of vortex-based compressor design configuration are illustrated along Plane 1. (a) Volume fraction of water, (b) velocity streamline, and (c) static pressure.

Following the discussion of the first results, the industry partner, Carnot Compression, suggested performing numerical simulations using boundary conditions followed.

- Rotational speed: 2200 RPM.
- Air Inlet is assigned with the mass flow rate of 182.4 g/s with the volume fraction of [water, air] = [0.495, 0.505].
- Air Outlet relative pressure: 280,000 Pa.
- Water Inlet mass flow is assigned with the mass flow rate of 118.4 g/s with the volume fraction of [water, air] = [0.495, 0.505].
- Water Outlet relative pressure: 80,000 Pa.

Results obtained from the CFD calculations for the updated boundary conditions are depicted in Figures 6 and 7. The results were presented and discussed with the industry partner. It is concluded that the flow

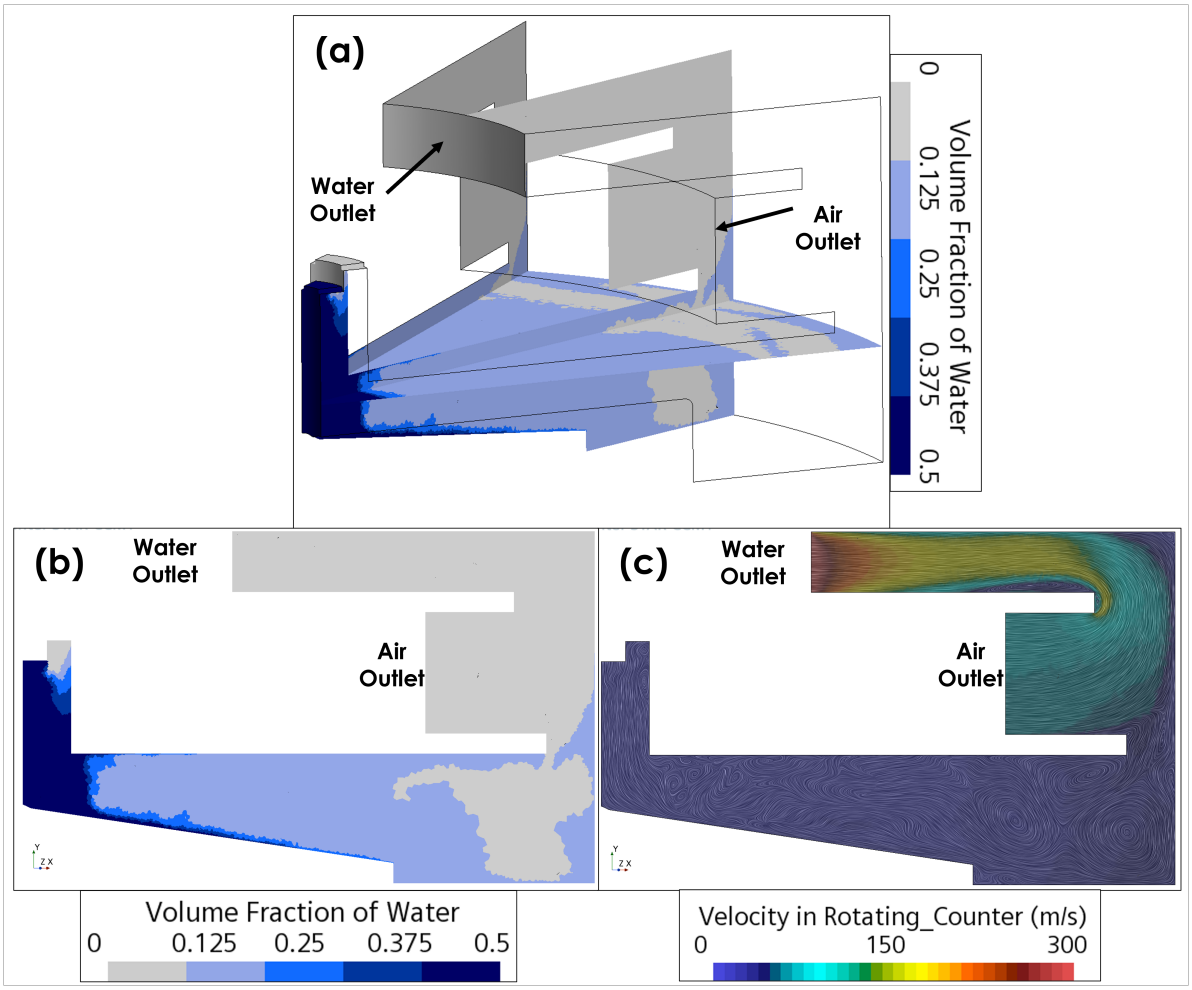

Figure 5. Results obtained from CFD calculations of the 1/6th domain of vortex-based compressor design configuration are illustrated along Plane 1 and Plane 2. (a-b) Volume fraction of water and (c) velocity streamlines along Plane 2.

behaviors revealed by CFD calculations are reasonably realistic. Based on the current design used for CFD calculations, a test facility of vortex-based compressor design is built and tested by Carnot Compression to obtain experimental measurements that will inform the feasibility and performance of the studied compressor design. After this analysis, the project was completed with the intention to begin a new CRADA with Carnot Compression to complete the intended analyses.

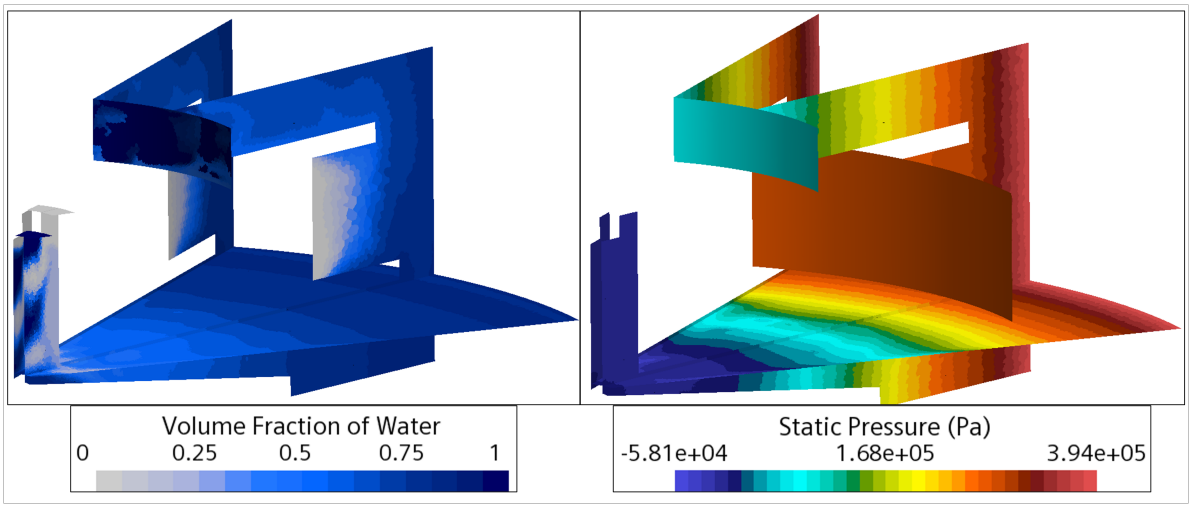

Figure 6. Results obtained from CFD calculations of the 1/6th domain of vortex-based compressor design configuration are illustrated along Planes 1 and 2. (Left) Volume fraction of water and (right) static pressure. The water inlet and air inlet are assigned with predetermined volume fraction of water and air accordingly to the provided boundary conditions of [water, air] = [0.495, 0.505].

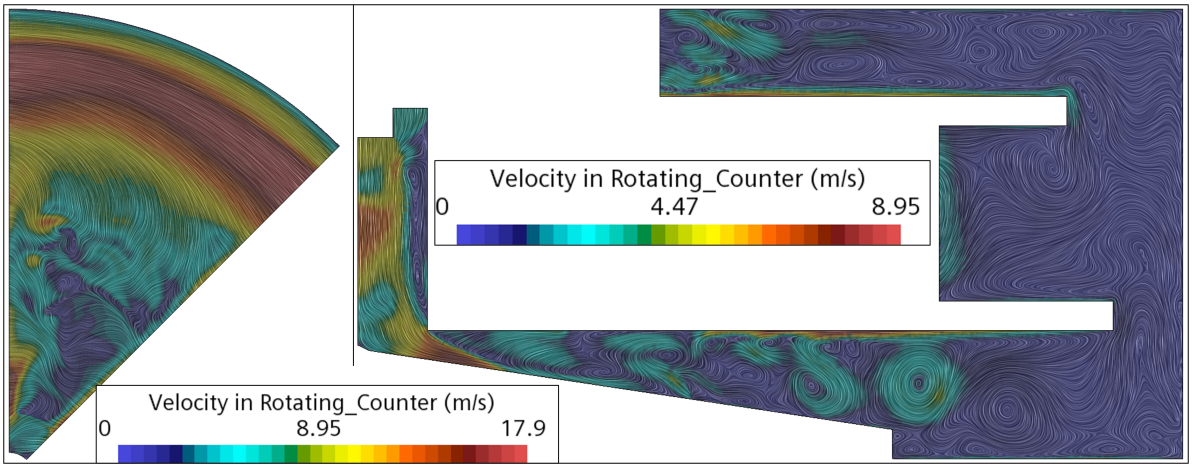

Figure 7. Results obtained from CFD calculations of the 1/6th domain of vortex-based compressor design configuration are illustrated along Planes 1 and 2. (Left) Velocity streamlines along Plane 1 and (right) along Plane 2, color contour shows velocity magnitude. The water inlet and air inlet are assigned with a predetermined volume fraction of water and air according to the provided boundary conditions of [water, air] = [0.495, 0.505].

4. CONCLUSIONS

During the CRADA project execution, Carnot Compression developed several compressor designs and requested technical assistance from ORNL to perform numerical modeling of those configurations. Two main configurations of compressors are the vortex and lambda designs, each with several minor modifications done by Carnot Compression during the project execution. For this CRADA period, the ORNL team provided support for numerical modeling for the vortex-based compressor design configuration. Using the compressor's CAD design and operating and boundary conditions provided by Carnot Compression, the ORNL team successfully performed numerical studies of the 1/6th domain of a vortex-based compressor design configuration. For this modeling effort, the RANS realizable k-ϵ turbulent model was applied and the segregated flow and segregated multiphase temperature models were selected to model the energy and flow transport. The obtained CFD results were shared and discussed with the industry partner on a regular basis (emails and biweekly meetings). Based on the outcomes from CFD calculations, minor changes to the compressor designs and operating conditions were made. At the end of this CRADA, Carnot Compression shared experimental results acquired from the vortex-based compressor design and confirmed that this configuration does not provide sufficient air pressure. The industry partner decided to switch the ORNL technical support to the lambda-based compressor design configuration.

5. ACKNOWLEDGMENTS

This material is based upon work supported by the US Department of Energy, Office of Energy Efficiency and Renewable Energy, Building Technologies Office under Contract No. DE-AC05-00OR22725. The authors would like to acknowledge Tony Bouza, BTO technology manager for HVAC&R, water heating, and appliances.

6. REFERENCES

Jones, W Peter, and Brian Edward Launder. 1972. "The prediction of laminarization with a two-equation model of turbulence." *International Journal of Heat and Mass Transfer* 15 (2): 301–314.

Rodi, Wolfgang. 1991. "Experience with two-layer models combining the k-epsilon model with a one-equation model near the wall." In *29th Aerospace sciences meeting,* 216.

Shih, Tsan-Hsing, William W Liou, Aamir Shabbir, Zhigang Yang, and Jiang Zhu. 1995. "A new k-epsilon eddy viscosity model for high Reynolds number turbulent flows." *Computers & fluids* 24 (3): 227–238.

User Guide, Star-CCM+. 2021. "StarCCM+ version 2021.1." *SIEMENS simcenter.*